Published in final edited form as:
*Biomed Mater*. 2008 September ; 3(3): 034110. doi:10.1088/1748-6041/3/3/034110.

# Generation of an artificial skin construct containing a non-degradable fiber mesh: a potential transcutaneous interface

**Frederick Cahn**[1] and **Themis R Kyriakides**[2,3]

1 *Biomedical Strategies Inc., San Diego, CA, USA*

2 *Vascular Biology and Therapeutics, Yale University, New Haven, CT 065356-9812, USA*

3 *Departments of Pathology and Biomedical Engineering, Yale University School of Medicine, New Haven, CT 065356-9812, USA*

## Abstract

Generation of a stable interface between soft tissues and biomaterials could improve the function of transcutaneous prostheses, primarily by minimizing chronic infections. We hypothesized that inclusion of non-biodegradable biomaterials in an artificial skin substrate would improve integration of the neodermis. In the present study, we compared the biocompatibility of an experimental substrate, consisting of collagen and glycosylaminoglycans, with commercially available artificial skin of similar composition. By utilizing a mouse excisional wound model, we found that the source of collagen (bovine tendon versus hide), extent of injury and wound contraction were critical determinants of inflammation and neodermis formation. Reducing the extent of injury to underlying muscle reduced inflammation and improved remodeling; the improved conditions allowed the detection of a pro-inflammatory effect of hide-derived collagen. To eliminate the complication of wound contraction, subsequent grafts were performed in guinea pigs and showed that inclusion of carbon fibers or non-degradable sutures resulted in increased foreign body response (FBR) and altered remodeling. On the other hand, inclusion of a polyester multi-stranded mesh induced a mild FBR and allowed normal neodermis formation. Taken together, our observations suggest that non-degradable biomaterials can be embedded in an artificial skin construct without compromising its ability to induce neodermis formation.

### Keywords

artificial skin; biomaterials; transcutaneous prosthesis; foreign body response

## 1. Introduction

Current prosthetics for orthopedic amputation patients suffer numerous problems, mainly at the stump–socket interface. Implantation and osteointegration of the load-bearing shaft directly into bone can provide a solution to these problems, since mechanical stress is transmitted directly to the bone, a tissue that is better suited to handle it. Clinical studies of osteointegrated prosthetics have demonstrated these advantages; these devices also provide superior control, range of motion and perception [1]. However, osteointegrated prosthetics must penetrate the skin of the stump and there has been no satisfactory method for a medical device to penetrate the skin permanently and without chronic inflammation and frequent infection. This problem

E-mail: E-mail: themis.kyriakides@yale.edu.

has been a serious drawback to osteointegrated prosthetics, preventing widespread regulatory approval and clinical use.

Permanent penetration of the skin with biomaterials is an unsolved clinical problem, for example in-dwelling catheters used require frequent replacement, in spite of the many recent technical improvements such as anchoring devices and antimicrobial coatings. Foreign body responses leading to inflammation and marsupialization of the epidermis remain a characteristic biological response, leading inevitably to microbial colonization and formation of biofilms on the biomaterial which are highly resistant to treatment [2]. For catheters, the clinical solution is replacement; however, for osteointegrated devices, this is not a practical option.

Recent clinical progress has reduced the incidence of infections in osteointegrated prosthetics: a key improvement in the surgical protocol restricts skin motion around the abutment exiting the residual limb by reflecting tissue away from the bone so that the skin can adhere directly to it [1].

Another insight into the problem of long-term penetration of the skin was the observation that the pedicle of the deer antler is tightly anchored to the dermis by the porous morphology of the bone surface and by collagen fibers extending radially from the bone [3]. This observation led to a design for a transcutaneous osteointegrated pin design that includes a flange and porous coatings for attachment of the dermis that was successfully demonstrated in a goat model [3].

However, the skin/device interface of the existing technology does not provide an ideal transfer to the device of mechanical stresses caused by the normal motions of the surrounding skin because of the rigid nature of the flange due to the formation of scar tissue, and the effectiveness of this design in a demanding setting, such as the lower leg limb, has not been demonstrated.

Our approach includes two novel elements: a dermal anchor device that is not rigid and which has controlled mechanical compliance in order to minimize mechanical stress at the abutment/device interface as well as at the skin/device interface, and the embedding of the dermal anchor in an artificial skin scaffold that is capable of regenerating dermal tissue without scar formation after implantation.

As a first step in engineering this dermal anchor, we hypothesized that the resorbable scaffold of clinically proven artificial skin could be modified to include embedded non-degradable biomaterial fibers without disrupting the formation of neodermal (non-scar) tissue. After the neodermis is formed and the wound is definitively closed by epidermis, fibers would be integrated with the neodermis and able to transfer force from the skin. However, the presence of non-degradable polymeric fibers could alternatively lead to enhanced foreign body response (FBR) and alter the remodeling process in the direction of scar tissue formation.

The FBR is elicited by biomaterials and involves the formation of foreign body giant cells and the deposition of a dense network of collagenous fibers [4]. In addition, the FBR limits neovascularization and could reduce the viability of cells within the neodermal tissue. In the present study, we first compared the neodermis formation of our artificial skin with that of the commercially available product in a mouse wound healing model. Subsequently, we generated artificial skin containing biomaterials such as non-degradable fibers and mesh as prototypes and examined their biocompatibility in a guinea pig wound healing model. We were able to find design parameters for the biomaterial fibers that did not alter neodermis formation or neovascularization, suggesting that it is feasible to engineer a transcutaneous post-skin interface.

## 2. Materials and methods

### 2.1. Commercial control artificial skin

Sheets of commercial artificial skin (125 $cm^2$) were purchased from Integra Lifesciences Corporation (Plainsboro, NJ) (Item number IAS4051, lot 4600110C) and served as commercial control. This product is aseptically processed and packaged in 70% isopropanol. It was cut into 1 × 1.5 $cm^2$ pieces for the animal experiments and stored at 4°C in 70% isopropanol.

### 2.2. Laboratory artificial skin

The following materials were used in the manufacturing process for laboratory-made artificial skin. Semed F fibrous collagen powder, derived from bovine hide (lot 37942) was purchased from Kensey Nash Corporation, Exton, PA. Chondroitin-6-sulfate (Cat. SAM-5EN-100, lot N-272) was purchased from Seikagaku America, East Falmouth, MA. Bovine deep flexor tendons were purchased from Lampire Biological Laboratories, Inc., Pipersville, PA. Glutaraldehyde (25%, w/v) was purchased from Sigma-Aldrich, St Louis, MO (Grade 1, Catalog G5882). Silicone adhesive (Silastic® Medical Adhesive Type A, Dow Corning, lot 0001930398) was purchased from Factor II, Inc. (cat. A-100, Factor II, Inc., Lakeside, AZ). Crude ficin was purchased from Sigma-Aldrich, St Louis, MO (cat F6008). Water for injection ('WFI', Cat 24125-500, VWR International, Inc.) was used for process steps. Lyoguard® freeze-drying containers (Part no. LGT-32255) were purchased from W L Gore & Associates, Inc. Sutures were purchased from esuturees.com. Multi-stranded 840 denier polyester yarn was obtained from NovaComp, Inc. (Willow Grove, PA).

### 2.3. Knitted polyester fabric

A plain single jersey knitted mesh fabric with a pore size of 400 $\mu$m was made from polyester yarn/filaments of 840 denier using a Master Sampler Electronic Circular Single Jersey m/c. The machine specifications are 10 inches diameter, 3 feed, 18 cut, 564 needles. The mesh was washed with cold water and scoured and bleached at a temperature of about 92.5°C, for 10 min. The fabric sample was then dried and stabilized by heat setting at 130°C with an iron. Care was taken to avoid direct contact of iron with the sample. Prior to use, the fabric was washed with ethanol and cut into appropriate size pieces.

### 2.4. Alkali-treated tendon collagen

Alkali-treated tendon collagen was prepared using a scalable process (US Patents 3520402 and 5019087). Sections of bovine deep flexor tendon, freshly harvested, were mechanically cleaned off fat, fascia and other extraneous matter, and then washed with a 2% sodium dodecyl sulfate solution. The ends were removed and the tendon sections were sliced (0.5 mm thick). Sections were suspended in 700 mL potassium phosphate monobasic (5 g $L^{-1}$, pH 6.3). 64 mg of the proteolytic enzyme ficin (cat F6008, Sigma-Aldrich, St Louis, MO) was added and the mixture was incubated with occasional stirring for 1 h at 37 °C. The enzyme solution was decanted from the tendon slices and was replaced with enzyme neutralization buffer (1% w/v ammonium nitrate and 0.1% w/v sodium chlorite). The tendon slices were then incubated at RT in a laminar hood for 48 h in a solution of 5% (w/v) sodium hydroxide and 20% (w/v) sodium sulfate. The alkali mixture was neutralized on an ice bath with 1 N sulfuric acid in 20% (w/v) sodium sulfate. The collagen was extensively washed with distilled water adjusted to 4.6 (approximate isoelectric point of alkali-treated collagen) with HCl. After washing, collagen preparations were compressed to a cake and stored at −20 °C. Samples were analyzed for helical content by Fourier transform infrared (FTIR) spectroscopy.

### 2.5. Preparation of laboratory control artificial skin

The laboratory-made artificial skin test articles ('lab control') were prepared as described previously [5]. Briefly, suspensions of 0.5% (w/v) fibrous collagen were prepared by adding collagen to 50 mM acetic acid in WFI. The mixture of acid-soluble collagen and acetic acid was blended at low speed to disperse and hydrate the collagen, and then homogenized with a Ross mixer for 20 min. The chondroitin-6-sulfate solution was slowly added, over 10 min, to the collagen dispersion, which was kept below 15 °C. The formed precipitate was observed as a large decrease in the viscosity of the suspension and was degassed under high vacuum. 12 mL aliquots of the collagen-chondroitin-6-sulfate mixture were poured into 6.5 cm diameter Lyoguard® and cooled following an optimized freezing rate for our equipment, and a lyophilization program that allowed the generation of uniform, sponge, without freeze pattern or cracking. These steps are important for determining the average pore size, one of the critical quantitative parameters affecting the biological activity of artificial skin [6]. Following lyophilization, sponges were placed in a vacuum oven at 105 °C for 2 days and allowed to cool under vacuum for an additional day. This dehydrothermal crosslinking step [7] creates an initial cross-linking of the dry sponge to preserve its porosity and prevent collapse upon rehydration [18].

A Gardner blade was used to prepare a silicone film of a nominal thickness of 0.25 mm on a polyethylene film placed over a sheet of a plate glass plate. The sponges were retrieved in a laminar flow hood and pressed into a silicone film and then overlaid with a second glass plate (covered with another sheet of polypropylene), separated by 1.52 mm thick nylon washers. The sponges were left under the hood for approximately 3 days, after which they were hydrated overnight using 50 mM acetic acid. The sponges were then cross-linked by soaking for 24 h at RT in airtight polycarbonate beakers containing 0.25% (w/v) glutaraldehyde in 50 mM acetic acid. Sponges were washed four times with WFI in individual beakers with agitation every 15 min for 1 h. After the wash cycles, each sponge was cut into 1.0 × 1.5 $cm^2$ rectangles and stored at 4°C in 70% isopropanol.

### 2.6. Preparation of sponges with imbedded fibers or meshes

14 mL of chondroitin-6-sulfate/bovine collagen dispersion was overlaid onto 24 inch segments of fiber or mesh material in individual Lyoguard® freeze-dry trays. The polyester mesh material was kneaded in the collagen-GAG suspension to insure that the fibers were coated with the suspension, and weighted to assure that they would lie at the bottom of the Lyoguard. This is the side of the sponge that will be in contact with tissue. The remainder of the processing was identical to that of the laboratory control artificial skin.

### 2.7. Analytical methods

**2.7.1. Helical content of collagen by FTIR spectroscopy—**A sample of dispersion was air dried in a weighing boat and the film was analyzed by transmission Fourier transform infrared (FTIR) spectroscopy to determine the helical content, i.e. the degree of denaturation of the collagen samples.

**2.7.2. Pore size by SEM and stereology—**Scanning electron microscopy (SEM) was carried out at the Nanotechnology User Facility of the University of Washington. Random fragments of lyophilized and dehydrothermal cross-linked sponges were obtained and coated with 5 nm of gold/palladium. All images were taken at a 90° tilt at 100, 250 and 500 × magnification. The average pore size was measured by stereology from scanning electron micrographs by drawing reference lines of measured length on the photographs and counting the number of crossings of the pore edges, and using the relationship [8]

$$L = \sum l_i / N.$$

**2.7.3. Endotoxin levels—**Samples (1 × 1.5 $cm^2$) of artificial skin were submitted to the University of Washington Engineered Biomaterials (UWEB) testbed center for endotoxin testing by a Gel Clot endpoint LAL assay (Cambrex) with an endpoint sensitivity of 0.06 EU. Each sample was extracted with 1 mL water. All samples were negative for endotoxin.

**2.7.4. Artificial skin grafts—**Animal surgery and husbandry were performed in the facilities of Perry Scientific, San Diego, CA. C57Bl6 mice at 3 month of age weighing approximately 25 g were used in these experiments. Full-thickness (down to but not including the subdermal *panniculus carnosus* muscle tissue) excisional wounds (1 × 1.5 $cm^2$) were made on the dorsal region of mice and either commercial or laboratory-made artificial skin was sutured in place and its effects on wound healing were evaluated 14 days later. A total of six mice per group were utilized. Hartley guinea pigs, 1–2 months of age, weighing 400–500 g each, were randomly assigned to groups containing an appropriate number of animals per test article and housed in large cages, four in a cage. A total of six guinea pigs per group were utilized. Guinea pigs were shaved and residual hair removed with a commercial depilatory (Nair®) the previous day or the morning of the study. Tetracycline was given subcutaneously at a dose rate of 0.1 mg $kg^{-1}$. The guinea pigs were anesthetized using halothane at a concentration of 2.5%. An incision using a #10 surgical blade was made around the perimeter of a 1.0 × 1.5 $cm^2$ graft area down to the *panniculus carnosus* without cutting into it. The dermal tissue within the perimeter was excised with the blade. The artificial skin was placed in the recipient site and sutured in place using 5-0 Ethicon suture (ten per graft). Graft sites were covered with a sterile sponge and two wraps of elastoplast. Grafts were examined at periodic intervals and bandaged again if necessary until the animals were terminated. At 17 days following surgery, the animals were euthanized and the graft site including 2–5 mm of normal surrounding tissue was removed.

### 2.8. Histology and immunohistochemistry

Harvested tissues were placed in 10% formalin, processed and embedded in paraffin to generate sections. Sections were stained with hematoxylin and eosin (H&E) and Masson's trichrome according to standard protocols. Slides were also stained with anti-PECAM-1 antibody (BD Bioscience-Pharmingen) to visualize blood vessels and anti-F4/80 and Mac3 antibodies (Abcam) to visualize macrophages as described previously [9,10]. The bound primary antibodies were detected by using the perodixase-based ABC Elite kit (VECTOR Laboratories). The sections were counterstained with 1% methylene green for 2 min and mounted. All slides were examined with the aid of the Nikon Eclipse microscope.

## 3. Results

### 3.1. Characterization of an artificial skin construct

FTIR spectroscopy revealed a spectrum at 8 $cm^{-1}$ resolution from 4000 to 600 $cm^{-1}$ (figure 1 (*C*)). The peak height was measured at 1450 $cm^{-1}$ above the baseline between 1360 and 1485 $cm^{-1}$ as well as the peak height at 1235 $cm^{-1}$ above the baseline between about 1170 and 1300 $cm^{-1}$. The measured $A_{1235}/A_{1450}$ ratio was 1.18; the ratio for non-denatured collagen should be 1.1 or above. Consistent with previous analysis of non-crosslinked collagen, the peaks at 1450 $cm^{-1}$ and 1235 $cm^{-1}$ are amide II and amide III, respectively [11]. Peak II represents N–H bond bending and C–N bond stretching. Peak III at 1235 $cm^{-1}$ represents multiple bonds that include C–C, N–H and C–N.

Determination of the pore size from SEM images indicated pore sizes with diameters in the range of 115–120 $\mu$m, which are within the optimum range of about 50–150 $\mu$m [12] (figure 1).

### 3.2. Biocompatibility of artificial skin in mice

Overall, both grafts induced inflammation and underwent remodeling predominantly in the areas of interaction with surrounding tissues such as the edges and underlying tissue (figure 2). Host cells invaded the grafts and were distributed throughout the scaffold area. The commercial artificial skin control elicited a favorable healing response that consisted of invading cells and loosely organized extracellular matrix. The scaffold was integrated with the surrounding tissue but maintained its original architecture. Histological evidence of scar formation was not observed in this model. Increased inflammation and ECM deposition were observed in the experimental graft (figures 2(*B*), (*C*)). Masson's trichrome stain was performed to analyze the extent of remodeling within the scaffolds, which was more extensive in the experimental scaffold (figure 3(*B*)). Only a portion of the scaffold located at the apical surface was not extensively remodeled. In contrast, remodeling in the commercial artificial skin scaffold was limited and the original architecture of the scaffold was maintained (figure 3 (*A*)). Consistent with the excessive remodeling, an abundance of foreign body giant cells (FBGC) and inflammatory cells was observed in the experimental scaffold. Inflammation was also evident in the commercial scaffold but was more limited.

Histochemical and immunohistochemical analyses of the cellular component of the two scaffolds revealed differences in overall invasion and inflammation. Enumeration of all nucleated cells, including FBGC, revealed a significant increase in the cell content of the experimental scaffold (figure 4(*C*)). Detection of macrophages, a major inflammatory cell type, with Mac3 antibody indicated that the increase in total cellularity was mirrored in the macrophage content (figure 4(*A*)). Quantification of macrophages, measured as the number of positive cells per high power field, confirmed the qualitative observations (figure 4(*D*)). Utilization of a second macrophage-specific antibody, F4/80, yielded similar results (not shown).

Scaffolds displayed some variability in cellular invasion and scaffold remodeling, an observation that prompted us to examine the reaction of the surrounding tissue in greater detail. An obvious complication was wound contraction, which is common and pronounced in the mouse model. In addition, we detected an association between damage to underlying muscle and excessive remodeling, which was easily observed in the commercial scaffold grafts (figures 5(*B*)–(*D*)). Remodeling at the proximity of the injured muscle displayed thicker collagen fibers and numerous inflammatory cells (figure 5(*B*)). At the apical parts of the scaffold, away from the injured muscle, remodeling was reduced (figure 5(*C*)). However, in comparison to scaffolds grafted without injury, inflammation was greater.

In addition to the influence of wound contraction and injury on underlying tissues, the source of collagen was found to influence the extent of inflammation and remodeling. Specifically, preparation and grafting of additional experimental scaffolds based on either tendon or hide-derived collagen indicated that the former was less inflammatory and underwent decreased remodeling (not shown). However, due to contraction and variable levels of injury during grafting the results were highly variable. Because of the complexities presented by the mouse model, we opted to perform subsequent studies in guinea pigs. We reasoned that due to a larger size, damage to the underlying muscle could be avoided and contraction would be limited.

### 3.3. Biocompatibility of artificial skin in guinea pigs

Experiments were repeated and great care was taken to minimize damage to the underlying tissue resulting in decreased inflammation and reduced remodeling of the grafts. Under these conditions, the tendon-derived grafts were comparable to commercial artificial skin (figure 6). Specifically, cellular invasion was less pronounced than in the previous experiments where the grafts were made with the hide collagen. Significant parts of the grafts, especially in the apical region, contained a loosely organized extracellular matrix that resembled the commercial grafts. In addition, both types of grafts contained numerous blood vessels suggesting that they elicited neovascularization. Inflammation was present at levels comparable to those seen in our best grafts of commercial artificial skin in mice. Specifically, enumeration of Mac3 positive cells from high power images indicated similar levels between the commercial and experimental grafts ($7.6 \pm 2.5$ versus $8.5 \pm 3.2$, $n = 5$). Taken together, our findings suggest that the biocompatibility of our experimental artificial skin approached that of the commercial product.

### 3.4. Artificial skin with embedded biomaterials

Based on the findings in the mouse and guinea pig wound healing models, constructs were generated that included carbon fibers or various non-biodegradable sutures. We chose commercial suture materials for this initial experiment due to the presumed high quality and cleanliness of these materials. The following range of materials was embedded separately in our artificial skin constructs: Alcon black monofilament nylon 9-0; Ethicon black monofilament nylon 11-0, ‘Ethilon’; Davis Geck blue monofilament propylene 6-0, ‘Surgilene’; Ethicon light green braded polyester 5-0, ‘Mersilene’; Ethicon blue monofilament propylene 10-0, ‘Prolene’; Carbon fibers, ‘sized,’ Sparta, Inc., San Diego CA, and polyester multi-stranded yarn. Here we present our findings with carbon fibers, polypropylene sutures and yarn. Overall, the presence of carbon fibers and surgical sutures had a negative effect on the healing response. Specifically, both materials caused extensive inflammation and induced scaffold remodeling (figures 7(*A*), (*B*)). Most of the scaffold was replaced by a fibrotic reaction and in the case of carbon fibers the formation of FBGC was pronounced. None of the original architecture could be observed, suggesting that the foreign body response was detrimental to the graft.

### 3.5. Study of a multi-stranded polyester mesh

Scaffolds containing a multi-stranded polyester mesh were prepared and grafted in guinea pigs with one wound site receiving the scaffold with the yarn, and a second wound site on the same animal was grafted with either laboratory or commercial artificial skin as a paired comparative control. Similar to our previous observations, the commercial control graft induced minimal inflammation and underwent some remodeling predominantly in the areas of interaction with surrounding tissues (not shown). Incorporation of the polyester mesh caused a minimal alteration of the overall remodeling response, which was more prominent in the area between the fibers (figures 7(*C*)–(*E*)). In addition, inflammatory and FBGC were present in the vicinity of the mesh. In contrast, the apical areas of the graft retained the loose collagenous network that was evident in grafts lacking biomaterials. Despite the inclusion of the polyester mesh, the elicited response was remarkably similar to that elicited by the in-house-made grafts alone. Furthermore, the mesh appeared to integrate well in the collagenous network and did not cause damage to the surrounding tissues. There was also no indication that the polyester-containing grafts were going to de-adhere from the surrounding tissue. Therefore, we conclude that we were successful in generating a well-tolerated and stable skin graft containing an incorporated polyester mesh.

## 4. Discussion

An osteointegrated prosthesis is a structural system that can be attached to an amputee's surviving natural bone to provide a direct, load-bearing path through the skin to an external prosthesis. Our overall objective is to develop improved osteointegrated prosthesis. The enabling technology that would make such a system clinically useful is a solution to the problem of inflammation and infection at the junction of the transcutaneous component and the skin. We hypothesize that normal motions of the flesh constantly pull the epidermis away from its junction with the transcutaneous component, leading to the observed marsupialization of the epidermis, chronic inflammation and infection. To prevent this effect, a secure mechanical bond between the device and the dermis of the surrounding skin that could absorb mechanical stress and immobilize the dermal tissue below the junction of the epidermis and the device would be needed.

As a first step in engineering an anchor for the dermis, our objective in the present study was to obtain a stable integration of a non-degradable biomaterial fabric into the dermis. To create this junction and prevent scar tissue formation, we surrounded the anchor fabric with the collagen-GAG scaffold of artificial skin that is itself capable of regenerating dermal tissue without the formation of scar tissue [13]. Our results suggest that it is possible to incorporate a multi-stranded yarn into the regenerated dermis without compromising the quality of the regenerated dermis, and that the fibers are intimately associated with the new dermal tissue. There was an obvious difference in the FBR elicited by carbon fibers and sutures versus the yarn. At this time, we have no explanation for this observation. We believe that the much smaller diameters of the fibers within the multi-stranded mesh provide better biocompatibility than a monofiber of similar overall dimensions. The multifiber mesh also provides a more porous texture; texture is an important component of biocompatibility [14,15].

Similarly, we found that the two collagen preparations we used, hide- and tendon-derived, elicited different remodeling responses. Presumably, tendon-derived collagen might contain less impurities resulting in reduced inflammation and the formation of a more biocompatible scaffold. Another, not mutually exclusive possibility, is that the overall fibrillar arrangement and cross-linking of the tendon collagen render it less inflammatory. Consistent with this suggestion, previous studies have suggested that collagen composition and cross-linking can influence inflammation and remodeling [16].

One of the major limitations of our rodent wound repair models is that healing is dominated by contraction, making it difficult to observe the responses beyond about 2 weeks [17]. Switching from a mouse to a guinea pig model reduced but did not eliminate the contraction issue. As a consequence, we were unable to use epidermal autografts and carry the studies beyond 14–17 days. Long-term experiments with larger animals will be needed to further explore the feasibility of the dermal anchor. Furthermore, we observed an association between the extent of injury to underlying muscle and graft remodeling. This complication was difficult to avoid in the mouse model due to the thin layer of muscle under the dermis. Thus, controlling parameters such as source of collagen, wound contraction and surgical injury was found to be critical in limiting excessive remodeling.

Collectively, our studies suggest that non-degradable biomaterials, such as a woven mesh, can be incorporated in tissue-engineered substrates and do not interfere with proper tissue remodeling. It is possible that the presence of the dermal equivalent reduces the overall FBR. Based on our observations, we suggest that it might be possible to improve the FBR to some biomaterials by embedding them in substrates that are prone to induce tissue remodeling instead of scar formation.

Generation of neodermis in the presence of a multi-stranded yarn demonstrated that it is possible to obtain stable integration of a non-degradable biomaterial fabric into the dermis. Furthermore, our studies suggest that it is possible to engineer a functional interface between osteointegrated prostheses and surrounding skin.

## Acknowledgements

We thank Jonathan Parker and Leung Oi Yan for able technical assistance. We wish to acknowledge generous support from the National Institute for Child Health and Human Development under SBIR grant 1 R43 HD046303-01 (to FC). Mouse studies were supported by the US Army under SBIR contract W911NF-05-C-0016 to (FC).

## References

1. Brånemark R, Brånemark P, Rydevik B, Myers RR. J Rehabil Res Dev 2001 ;38:175–81. [PubMed: 11392650]
2. Elliott TS, Faroqui MH. Br J Hosp Med 1992 ;48:496–7. 500–3. [PubMed: 1422561]
3. Pendegrass CJ, Goodship AE, Blunn CW. Biomaterials 2006 ;27:4183–91. [PubMed: 16618500]
4. Anderson JM. Annu Rev Mater Res 2001 ;31:81–110.
5. Cahn, F. Methods of Tissue Engineering. Atala, A.; Lanza, RP., editors. San Diego: Academic; 2002 . p. 515-24.
6. Yannas IV, Burke JF, Warpehoski M, Stasikelis P, Skrabut EM, Orgill D, Giard DJ. Trans Am Soc Artif Intern Organs 1981 ;27:19–23. [PubMed: 7036496]
7. Yannas IV, Tobolsky AV. Nature 1967 ;215:509–10. [PubMed: 6057911]
8. Dagalakis NJ, Flink J, Stasikelis P, Burke JF, Yannas IV. J Biomed Mater Res 1980 ;14:511–28. [PubMed: 7400201]
9. Kyriakides TR, Zhu YH, Yang Z, Huynh G, Bornstein P. Am J Pathol 2001 ;159:1255–6. [PubMed: 11583953]
10. Kyriakides TR, Foster MJ, Keeney GE, Tsai A, Giachelli CM, Clark-Lewis I, Rollins BJ, Bornstein P. Am J Pathol 2004 ;165:2157–66. [PubMed: 15579457]
11. Douglas T, Haugen HJ. J Mater Sci: Mater Med 2008 ;19:2713–9. [PubMed: 18283534]
12. Yannas IV, Lee E, Orgill DP, Skrabut EM, Murphy GF. Proc Natl Acad Sci 1989 ;86:933–7. [PubMed: 2915988]
13. Stern R, McPherson M, Longaker MT. J Burn Care Rehabil 1990 ;11:17–3.
14. Campbell CE, von Recum AF. J Invest Surg 1989 ;2:51–74. [PubMed: 2487399]
15. Brauker JH, Carr-Brendel VE, Martinson LA, Crudele J, Johnston WD, Johnson RC. J Biomed Mater Res 1995 ;9:1517–24. [PubMed: 8600142]
16. Rothamel D, Schwarz F, Sager M, Herten M, Sculean A, Becker J. J Clin Oral Implants Res 2005 ; 16:369–78.
17. Truong AN, Kowal-Vern A, Latenser BA, Wiley DE, Walter RJ. J Burns Wounds 2005 ;4:e4. [PubMed: 16921409]
18. Yannas, IV., et al. Method for preserving porosity in porous materials . US Patent 4522753. 1985.

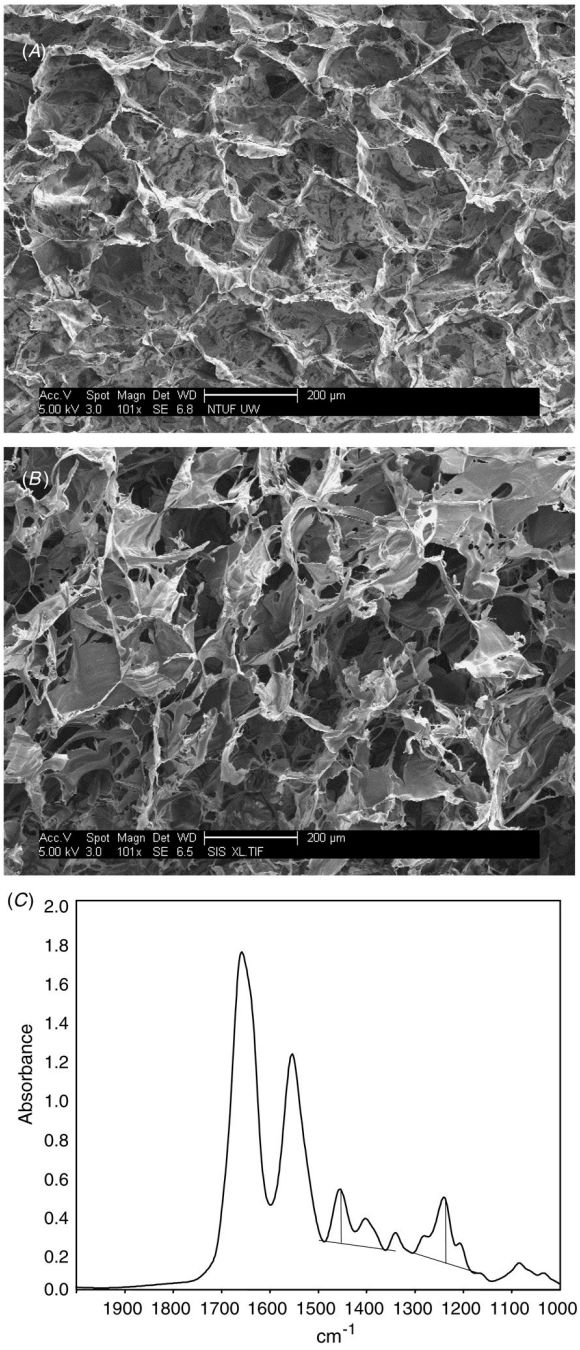


**Figure 1.**
Characterization of an artificial skin scaffold. Random SEM images of lyophilized and dehydrothermal cross-linked scaffolds made of collagen derived from Semed (*A*) or tendon (*B*) are shown. Both scaffolds displayed outstanding porosity. (*C*) FTIR spectroscopy shows the degree of denaturation of the collagen samples. Bar = 200 $\mu$m (*A*), (*B*).

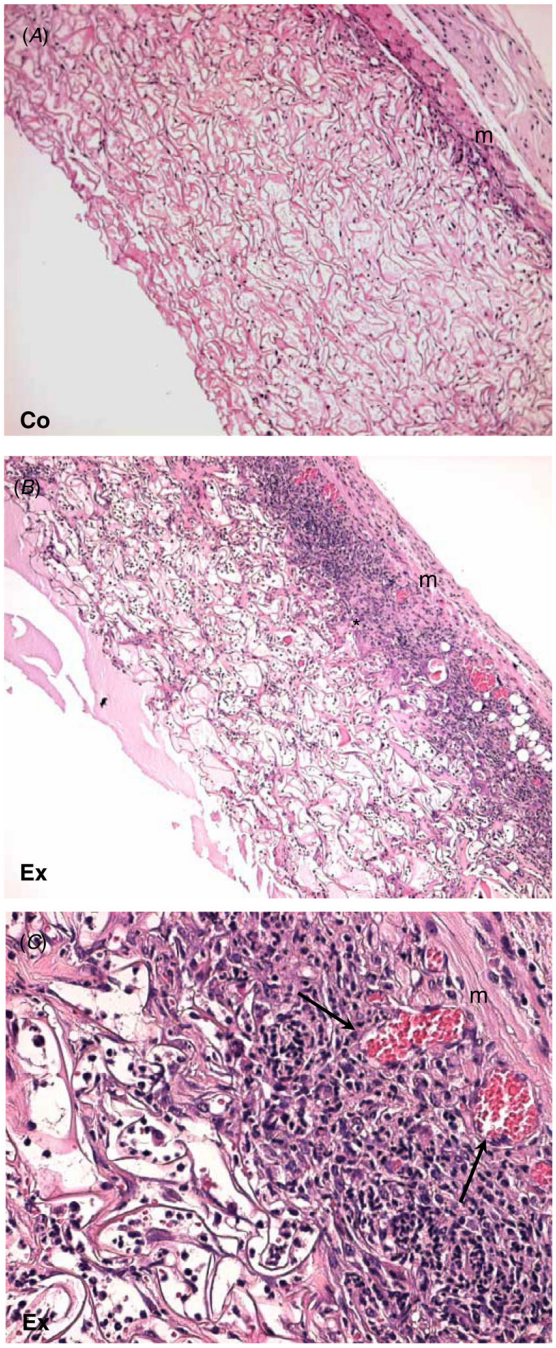


**Figure 2.**
Increased cellular invasion in tendon-derived grafts. Representative H&E-stained images of commercial (*A*) and experimental (*B*, *C*) artificial skin grafted in mouse wounds for 14 days are shown. (*A*) Commercial graft shows limited cellular invasion and normal interface with the underlying muscle (m). (B) Laboratory-made graft shows extensive cellular invasion and remodeling (*). (*C*) A higher magnification of (*B*), showing numerous inflammatory cells and blood vessels (arrows). Original magnification: 100 × (*A*), (*B*); 400 × (*C*).

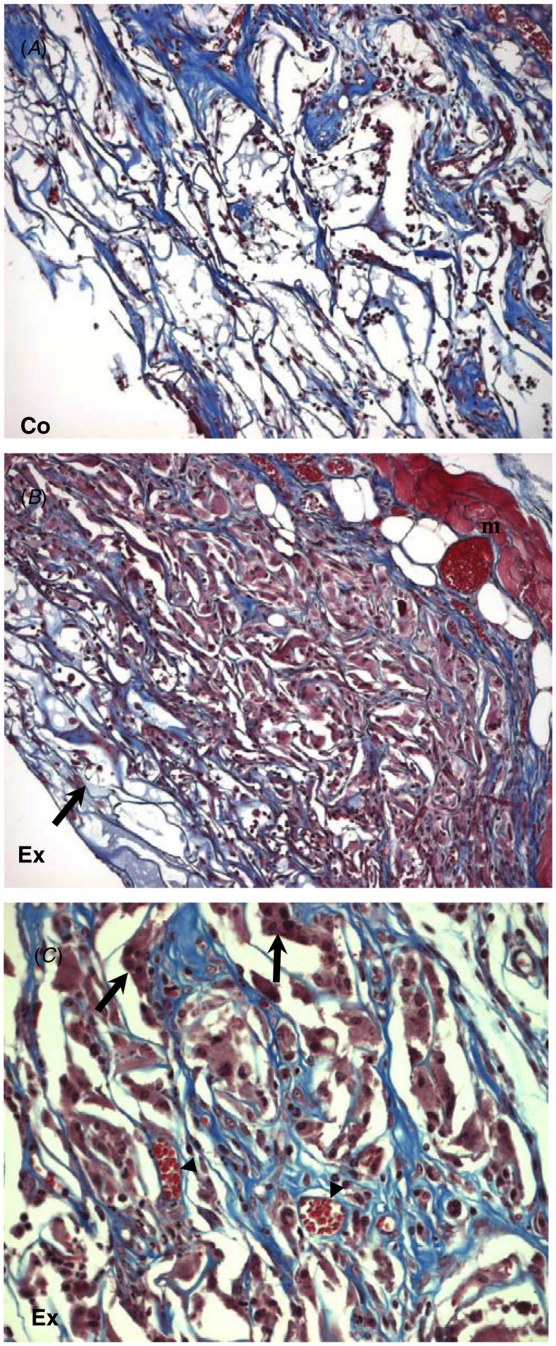


**Figure 3.**
Increased remodeling and matrix deposition in tendon-derived grafts. Representative images of Masson's trichrome-stained sections of laboratory-made (*A*) and commercial grafts (*B*, *C*) are shown. (*A*) Commercial artificial skin graft with normal cell invasion is shown. (*B*) A skin graft with excessive cell invasion and remodeling. Only a portion of the graft, situated closest to the apical surface, has not undergone extensive remodeling (arrow). The underlying muscle appears red and is labeled (m). (*C*) Higher magnification of (*B*) showing cellular invasion, including formation of FBGC (arrows), ECM remodeling and angiogenesis (arrowheads) can be observed. Limited cellular invasion, FBGC formation (arrow) can be observed in the non-remodeled scaffold (*C*). Original magnification: 100 × (*A*), (*B*); 200 × (*C*).

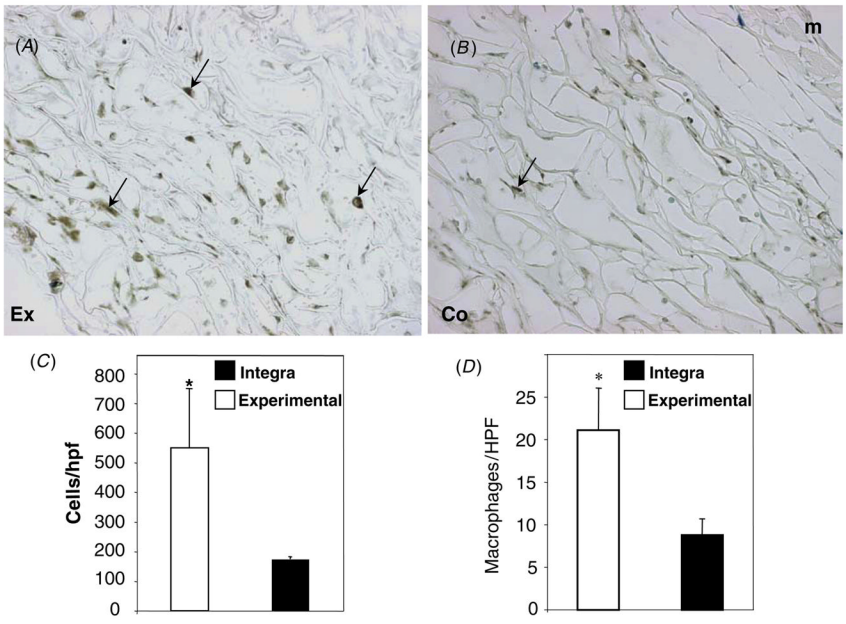


**Figure 4.**

Increased macrophage response in tendon-derived grafts. Representative images of sections stained with the macrophage-specific antibody Mac3 (*A*), (*B*) from laboratory-made (*A*) and commercial (*B*) artificial skin grafts and visualized with the peroxidase reaction (brown color). Experimental skin grafts displayed the increased presence of macrophages (arrows). Nuclei were counterstained with methyl green. Original magnification: 400 × (*A*), (*B*). (*C*) The total number of nucleated cells per high power field was determined by manual counts of 50 images per graft. (*D*) The number of macrophages (Mac3 positive) per high power field was quantified from 150 digital images from each graft. * $p$ value $\leq 0.05$.

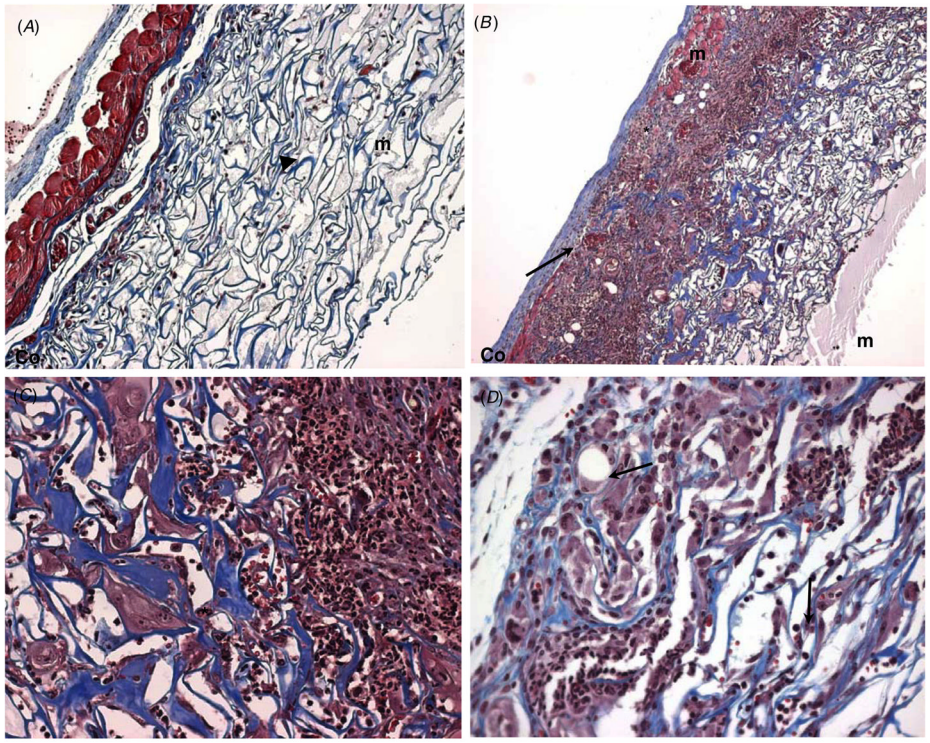


**Figure 5.**
Extensive of injury prevents neodermis formation. Representative images of Masson's trichrome-stained sections of commercial artificial skin grafted in mice for 14 days are shown. (*A*) A skin graft with normal cell invasion is shown. The underlying muscle (m) is stained red and is intact. Remodeling is limited to the basal layer of the scaffold (arrowhead) (original Magnification: 100 ×). (*B*) The area of graft that sustained muscle injury prior to grafting is shown. The edges of the injured muscle can be seen, marked as (m). Areas of excessive inflammation and remodeling can be observed (*). Increased thickness of the fibers in the scaffold (blue color) suggests active remodeling. The apical part of the graft showing less inflammation and remodeling is identified (arrow) (*C*) and (*D*). Higher magnification of image (*B*). (*C*) Image showing the transition from excessive inflammation to active remodeling (*). Extensive scaffold remodeling can be observed, fibers appear blue and display increased thickness. (*D*) The area of the graft near the apical surface displaying extensive cellular invasion and inflammation (arrows), but less remodeling. Original magnification: 100 × (*A*), (*B*); 200 × (*C*), (*D*).

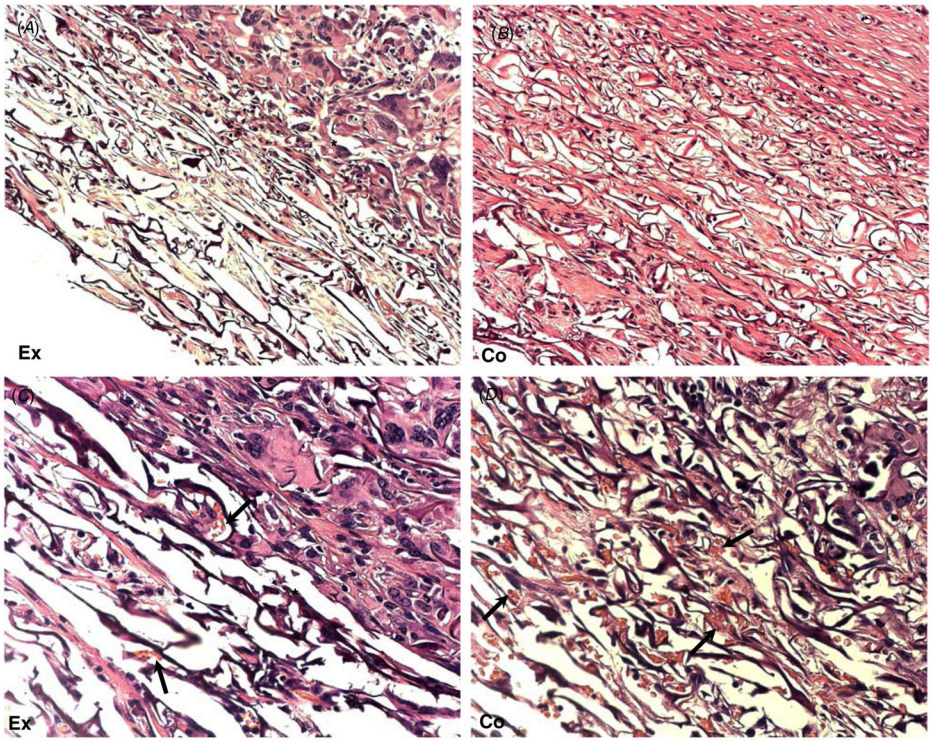


**Figure 6.**
Comparison of commercial and tendon collagen-derived laboratory-made grafts in a guinea pig model. Representative images of H&E-stained sections of laboratory-made (*A*), (*C*) and commercial artificial skin grafts (*B*), (*D*) implanted in guinea pigs for 17 days are shown. (*A*) Laboratory-made graft displaying both dense (*) and loose extracellular matrices. The latter is extensive and resembles the remodeling seen in the commercial graft in (*B*). (*B*) A commercial artificial skin graft displaying loose organization of the collagenous network, and no evidence of excessive inflammation is shown. Dense matrix organization can be observed at the most basal part of the graft (*). (*C*) and (*D*) Higher magnification of images (*A*) and (*B*), respectively, are shown. (*C*) Image of the experimental graft demonstrating the interface between dense (*) and loose extracellular matrices. In the latter, normal cellular content and numerous blood vessels (arrows) can be observed. (*D*) Image of the commercial artificial skin graft showing loose matrix organization and numerous blood vessels evident by the presence of red blood cells in vascular structures (arrows). Original magnification: 200 × (*A*), (*B*); 400 × (*C*), (*D*).

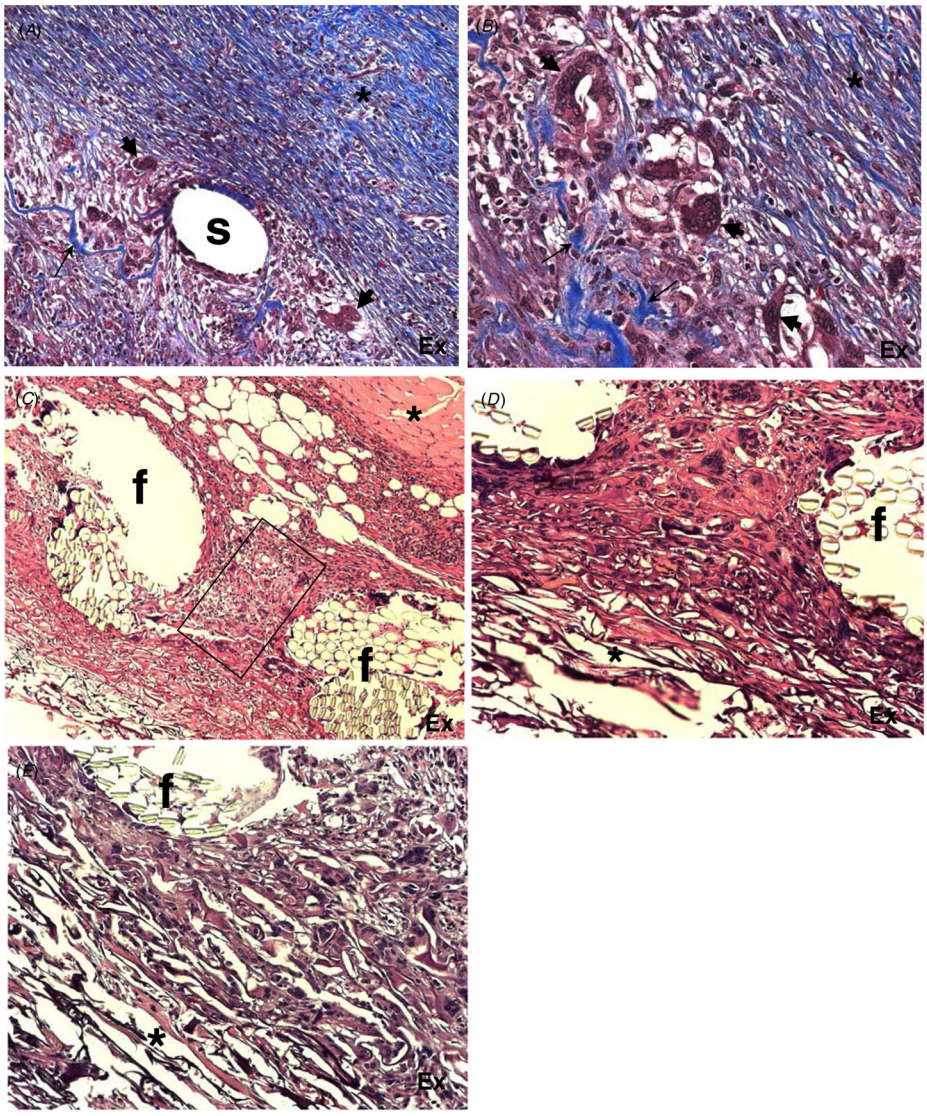


**Figure 7.**

Effects of carbon fibers, sutures and polyester mesh embedded in artificial skin grafts on the foreign body response. (*A*), (*B*) Representative images of Masson's trichrome-stained sections of experimental scaffolds embedded with polystyrene sutures (*A*) and carbon fibers (*B*) and grafted in guinea pigs for 17 days are shown. (*A*) The area surrounding polystyrene suture(s) showing extensive remodeling and deposition of a dense collagenous matrix (*) and FBGC formation (arrowheads). Remnants of the original graft can be observed as blue fibers (arrow). (*B*) The area surrounding a group of embedded carbon fibers (empty spaces) showing extensive remodeling and deposition of a dense collagenous matrix (*) and FBGC formation (arrowheads). Remodeling of the original graft can be observed as thick blue fibers (arrows). (*C*)–(*E*) Representative images of H&E-stained sections of experimental grafts containing a polyester mesh. (*C*) Low power image of the graft showing the complete integration of the mesh in the collagenous matrix. The underlying muscle layer (*) is undamaged. The rectangle denotes remodeled tissue in the interstitial space between mesh fibers (f). A loose extracellular matrix can be observed in the most apical part of the graft. (*D*)–(*E*) High power images of the polyester fiber (f) graft interface. The overall normal cellular content and loose extracellular

matrix can be observed in the proximity of the mesh (*). Original magnification: 100 × (*A*), (*C*); 400 × (*B*), (*D*), (*E*).